Spring 1-1-2018

Modeling of Fiber Microbuckling in Soft Composites Under Bending

Savina Brachthauser Balcells
University of Colorado at Boulder, brbalcells@gmail.com

Modeling of fiber microbuckling in soft composites under bending

by

Savina Brachthauser Balcells

B.S., Polytechnic University of Catalonia, 2015

A thesis submitted to the

Faculty of the Graduate School of the

University of Colorado in partial fulfillment

of the requirements for the degree of

Master of Science

Department of Ann and H.J. Smead Aerospace Engineering Sciences

2018

This thesis entitled:
Modeling of fiber microbuckling in soft composites under bending
written by Savina Brachthauser Balcells
has been approved for the Department of Ann and H.J. Smead Aerospace Engineering Sciences

Prof. Francisco Lopez Jimenez

Prof. Kurt Maute

Prof. Rong Long

Date

The final copy of this thesis has been examined by the signatories, and we find that both the content and the form meet acceptable presentation standards of scholarly work in the above mentioned discipline.

Brachthauser Balcells, Savina (M.S., Aerospace Engineering)

Modeling of fiber microbuckling in soft composites under bending

Thesis directed by Prof. Francisco Lopez Jimenez

Soft fiber reinforced composites are very suitable materials for space deployable structures. These materials are characterized by a very compliant matrix that allows the fibers to highly deform so microbuckling under bending can appear without failure. This mechanism acts as a stress-reliever, so the material can be folded to very high curvatures without damage. However, the existing models are not able to accurately capture the mechanical behavior of these materials.

A new micromechanical model is proposed for this materials under bending. The model considers both the pre and post buckling regimes using a large strain formulation. The strain energy is calculated as the sum of the energy in the matrix and the fibers. The energy of the matrix is calculated using homogenization methods and the energy of the fibers is approximated using classical beam theory. The obtained energy model is a function of the position of the neutral axis, the buckling wavelength and a function that defines where buckling appears through the thickness. These parameters are calculated by minimizing the energy.

The results obtained from the theoretical model are compared with numerical simulations. The comparison shows good agreement for the pre-buckling regime but it does not predict well the curvature when buckling appears. The influence of some problem parameters such as the volume fraction and the shear modulus of the materials is also studied.

Contents

Chapter

Figures

Figure

Chapter 1

Background

1.1 Introduction

High strain composites have been widely used in the last decades in deployable space structures. The required characteristics of these type of structures usually involve compact packaging, mass efficiency and high reliability. High strain composites are very suitable materials for these purposes because of their capability to fold. The large difference of several orders of magnitude between the stiffness of the matrix and the fibers allows the material to achieve very high bending strains without failure. Because of the softer matrix, fibers are allowed to deform freely which leads to the microbuckling of the fibers that are highly compressed. Figure 1.1 shows this phenomenon on a specimen under bending.

Figure 1.1: Microbuckling in a soft matrix composite under bending. Taken from [1].

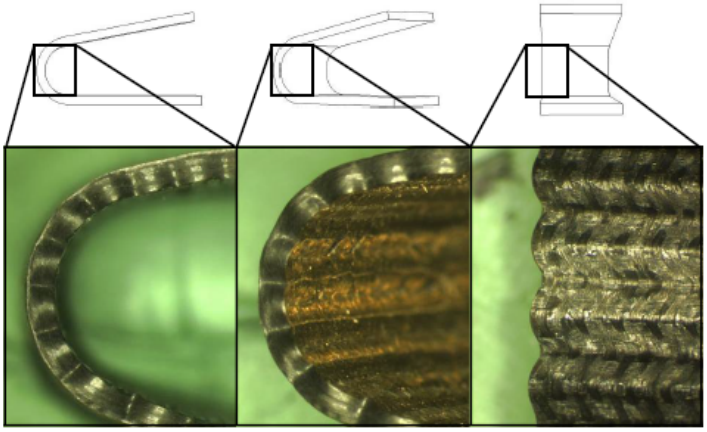

Such behavior, which does not appear in traditional fiber composites, is characterized by complex instabilities that are still difficult to model. The objective of the present work is to formulate a theoretical micromechanical model that will help to better understand the behavior of the material. This new approach is based on a large deformations formulation and homogenization methods applied to fiber reinforced materials.

An energy model has been developed based on the kinematics that have been experimentaly observed such as in the model presented by [1]. Following this approach, the strain energy of the composite is modeled as the sum of the matrix plus the fibers, which are calculated separately. Homogenization is used in order to obtain more accurate results, which leads to modeling the matrix as a Neo Hookean solid as was proposed in [2]. The resultant expression for the strain energy density is a function of some unknown kinematic parameters such as the wavelengths of the buckles. The strain energy is then minimized for this parameters.

A numerical model has also been developed to evaluate the theoretical model. The finite element method has been used to analyze a representative volume element of the material.

1.2 Motivation

The motivation of this work lies on the necessity of better understanding the mechanics of high strain composites for structural design purposes. These materials are commonly used in deployable space structures which are very diverse and usually have to meet very demanding requirements. Space structures in general are desired to be lightweight, resist space environment conditions and be highly reliable. Complex structures that are large in its operational configuration (antennas, solar panels, etc) need to fit small volumes during the launching phase. Deployable structures are needed for that purpose and high strain materials represent and alternative to traditional mechanical systems based on joints and motors according to [3]. High strain composites can be used in foldable structures that could

relay on its strain energy for deploying. Thus, the complexity and weight of the mechanisms that are usually used in this cases could be reduced.

Figure 1.2: Deployment of a truss structure. Taken from [4]

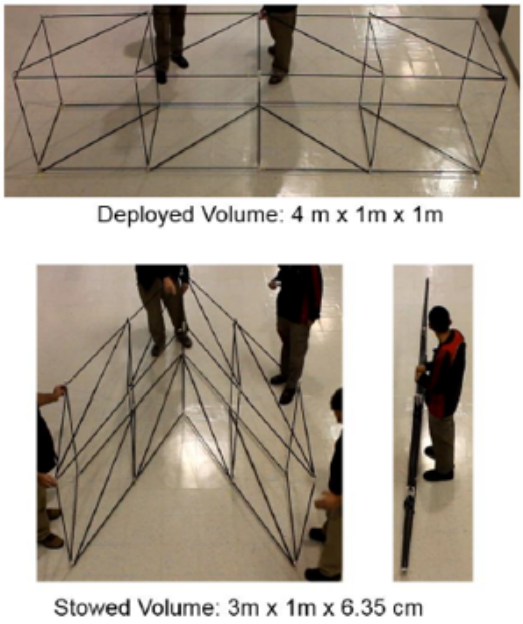

Several deployable systems based on this method are currently being developed and have already been tested as described in [3]. Examples include deployable booms, panels and truss structures for antennas, telescopes, solar sails, etc. Figures 1.2 and 1.3 show some applications. However, the behavior of these materials still needs to be further studied. A deep knowledge of the mechanics of the material is necessary to develop reliable and accurate models. In this context, this work aims to provide with a new analytical model that can help to understand the micromechanical instabilities that are characteristic of this material. A general parametric model has been developed so that it could be used for predicting the mechanical response of a high strain composite for some given material properties and for a certain bending curvature.

The influence of different factors such as the fibers distribution or the material properties are also studied by using the developed theoretical model. The purpose of this study is

Figure 1.3: Folding Sequence of a Composite Lamina in a Miura-Origami Pattern. The folding lines are made with Fiber-Reinforced High-Strain Matrix. Taken from [3].

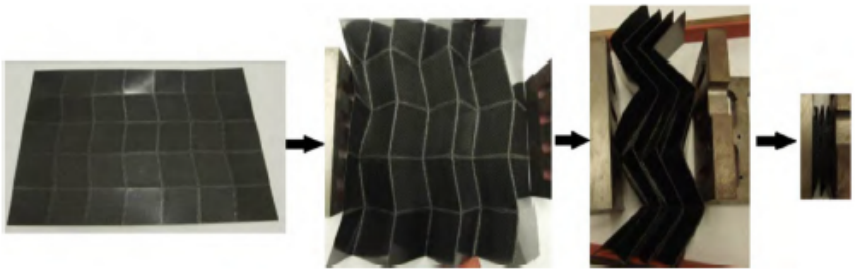

to try to determine when and why microbuckling occurs and what affects the length of the buckling waves. The obtained conclusions would help to quantify which factors dominate the response and what can be neglected. This is necessary in order to decide which assumptions can be made since a suitable model for design must be accurate and reliable but also as simple as possible to be functional.

1.3 Literature survey

1.3.1 Micromechanical models

Models based on micromechanics had been previously developed to study the failure of traditional composites due to microbuckling in compression. The first model that provided with an analytical solution was derived by [5]. The model extended the solution for buckling for a beam on an elastic foundation. He assumed two possible buckling modes which are described in figure 1.4. The difference between them is due to the matrix deformation: the first consists of a shear mode and the second is an extension mode. The shear mode turns out to be the less energetic so it is considered to be the preferred one. For both modes, compression is considered uniform and the amplitude and shape are constant through the entire thickness of the material.

Based on Rosen's model, many authors have further investigated the microbuckling

Figure 1.4: Rosen buckling modes

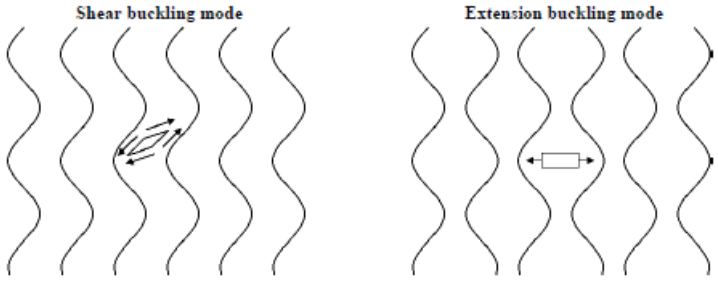

mechanisms in composites. Some of this work includes the identification of several buckling failure mechanisms in compression conducted by [6] and the efforts to predict the compressive strength and the influence of fiber volume fraction, material properties, fiber configuration, etc. such as the studies presented by [7], [8] and [9].

All the previous models only considered pure compression. For bending cases, those theories are not applicable anymore because the compression stresses are not constant and the microbuckling can not be assumed to be constant through the thickness. [10] describes how soft matrix composites behave when they are subjected to large bending deformations. Figure 1.5 shows how microbuckling appears in this case and how the stresses profile is shifted. After at a certain curvature the fibers reach their critical buckling load the compression stiffness is reduced in the post-buckled region. As a result, the neutral surface moves towards the tensile side of the material. This mechanism reduces the strains of the fibers and the matrix allowing the laminate to reach higher bending curvatures. While the figure shows the buckling in the bending plane, out of plane buckling is most commonly observed in experiments.

[10] derived the kinematics of the described systems and obtained the following expressions for the strains:

$$\epsilon_f = \pi^2 \frac{a_0 r_f}{l} \tag{1.1}$$

Figure 1.5: Fiber microbuckling in a soft composite under bending. Taken from [10].

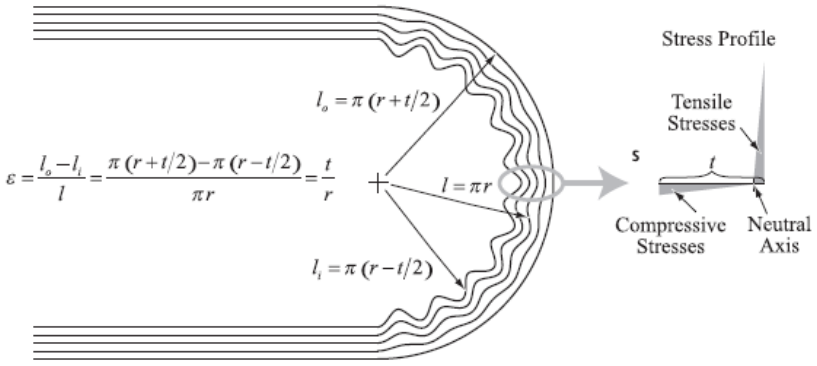

$$\epsilon = \left(\frac{l\epsilon_f}{2\pi r_f} \right)^2 \tag{1.2}$$

Where ϵ_f and ϵ stand for the fiber strain and the composite bulk strain. a_0, r_f and l are the amplitude of the buckles, the fiber radius and the buckling wavelength respectively. These expressions show that the microbuckling allows larger bulk material strains with smaller fiber deformations. Nevertheless, this expressions fails when trying to predict when microbuckling appears and the length of the buckles.

A micromechanical energy model that tries to adress this issues was developed by [1]. He proposes a strain energy model based on the kinematics observed in experiments. The model describes the post buckling behavior of the material under bending assuming that both the fibers and the matrix are incompressible. The energy is approximated by:

$$dU_t = dU_x + dU_{xy} + dU_{yz} + dU_f \tag{1.3}$$

U_x is the strain of the fibers that are under tension, U_{xy} and U_{yz} are the shear components of the composite that appear due to the microbuckling kinematics and U_f is the bending energy due to the microbuckling of the compressed fibers.

Strains are approximated based on the kinematics and assuming small displacements.

The resultant expression for the energy is a function of the bending curvature κ, the composite mechanical properties E_x,G_{xy} and G_yz, the fiber modulus E_f (material properties were experimentally determined), the material geometry (l,w,t,V_f,h and b) and the buckling wave length λ and the position of the neutral surface z_n:

$$U_t = \frac{1}{48}E_x lw(t-2z_{ns})^3\kappa^2 + \frac{1}{2}G_{xy}hw\kappa(\frac{t}{2}+z_{ns})^2 + \frac{G_{yz}wl\kappa\lambda^2}{4\pi^2}\ln\left(\frac{2(t+z_{ns})}{b}\right) + \frac{4\pi lwV_fE_fI_f}{h^2\lambda^2}\kappa(t+2z_{ns})^2 \tag{1.4}$$

It is assumed that after buckling appears, the strain energy of the fibers due to pure compression is neglected in comparison to the bending energy due to the buckling. Therefore, fibers are assumed to be inextensible. By applying several geometrical approximations, the expression for the buckling wave amplitude is found as:

$$a = \frac{2\lambda}{\pi}\sqrt{\kappa(z-z_{ns})} \tag{1.5}$$

The unknown terms in the total energy definition are analytically obtained by minimizing the energy and are found to be decoupled. The obtained expression for the neutral surface position reads:

$$z_{ns} = \frac{t}{2} + \frac{1}{\kappa}\frac{G_{xy}}{E_x} - \frac{1}{\kappa}\sqrt{\left(\frac{G_{xy}}{E_x}\right)^2 + 2t\kappa\left(\frac{G_{xy}}{E_x}\right)} \tag{1.6}$$

And the buckling wave length, which is assumed to be constant through thickness and also independent of the bending curvature, is approximated as:

$$\lambda = \frac{\pi}{2}\left(\frac{9V_ft^2d^2E_f}{8G_{xy}ln\left(\frac{6t}{d}\sqrt{\frac{V_f}{\pi}}\right)}\right)^{\frac{1}{4}} \tag{1.7}$$

This expression seems to be agree well with the experimental results that are provided. However, the moment derived from the strain energy exceeds the experiments by a factor of 1.9.

The previous model assumed linear elasticity, however it its clear that large deformations appear due to the microbuckling and high bending curvatures. Therefore, large strains formulation has been used for the model presented in this thesis in order to obtain more accurate results. Also, large strain formulations would allow to add material damage effects such as the Mullins effect ([11] and [12]).

1.3.2 Homogenization methods for fiber reinforced materials

Homogenization techniques are used for simplifying the description of the behavior of heterogeneous materials. In this case, the process consists on substituting the composite by a homogeneous solid that would have approximately the same macro mechanical behavior. The properties of the homogenized material are a function of the composite mechanical properties and its microstructure.

Since the proposed model is based on large deformations, nonlinear homogenization theory is necessary to describe the nonlinear regime for hyperelastic solids. Nonlinear homogenization has been already used in the last decades for modeling fiber composites under large deformations. Some examples include [13], [14] and [15].

[16] provides a homogenization constitutive theory for fiber-reinforced hyperelastic solids. By following an iterated homogenization procedure, a general solution that predicts the exact macroscopic response for a material with a random microstructure. Then, the closed form solution for a Neo-Hookean solid reinforced by anisotropic fibers is derived:

$$\tilde{W}_{SCC} = \tilde{\mu}_{HS}(I_1 - 3) + \frac{\tilde{\mu}_n - \tilde{\mu}_{HS}}{2} \frac{(\sqrt{I_4} + 2)(\sqrt{I_4} - 1)^2}{\sqrt{I_4}} \tag{1.8}$$

where:

$$\tilde{\mu}_n = (1 - V_f)\mu_m + V_f \mu_f \tag{1.9}$$

and:

$$\tilde{\mu}_{hs} = \frac{(1-V_f)\mu_m + (1+V_f)\mu_f}{(1+V_f)\mu_m + (1-V_f)\mu_f}\mu_m \tag{1.10}$$

Based on this solution, if the fibers are also modeled as Neo Hookean solids, the stored energy function becomes:

$$\tilde{W}_{IH} = \frac{\mu_{IH}}{2}(I_1 - 3) + \frac{\mu_n - \mu_{IH}}{2}\left(\frac{2}{\sqrt{I_4}} - 3\right) + \frac{\mu_n \mu_{HS}}{2} I_4 - \frac{\mu_{IH} - \mu_{HS}}{2}\frac{I_5}{I_4} \tag{1.11}$$

where:

$$\mu_{ih} = (1-V_f)^2\left(1 + \frac{2(2-V_f)V_f}{(1-V_f)^2}\frac{\mu_f}{\mu_m} + \frac{\mu_f^2}{\mu_m^2}\right)\frac{\mu_m}{2} - (1-V_f)^2\frac{\mu_f - \mu_m}{2} \tag{1.12}$$

$$\times\sqrt{\frac{2}{(1-V_f}\,)^2\frac{\mu_f}{\mu_m} + \left(1 + \frac{2(2-V_f)V_f}{(1-V_f)^2}\frac{\mu_f}{\mu_m} + \frac{\mu_f^2}{\mu_m^2}\right)} \tag{1.13}$$

I_1 is the first invariant of the Cauchy Green deformation gradient $C = F^T F$ and F is the deformation gradient whose components are obtained by differentiating the coordinates in the deformed configuration with respect to the undeformed one: $F_{ij} = \frac{dx_i}{dX_j}$ .I_4 and I_5 are functions of the deformation gradient and N, which is the vector that defines the fibers orientation.

$$I_1 = tr(C) \tag{1.14}$$

$$I_4 = N^T C N \tag{1.15}$$

$$I_5 = N^T C C N \tag{1.16}$$

Both I_1 and I_4 have a physical interpretation. I_1 corresponds to the sum of the principal stretches and I_4 is the stretch in the fibers directions. I_5 does not have physical meaning. For

the case in which fibers are not stretched, $I_4 = 1$ and therefore the strain energy equation becomes:

$$W_{IH}(I_4 = 1) = \frac{\mu_{IH}}{2}(I_1 - 3) - \frac{\mu_{IH} - \mu_{HS}}{2}(I_5 - 1) \tag{1.17}$$

The application of this method was already successfully tested by [2] for composites with fibers several orders of magnitude stiffer than the matrix. The strain energy was calculated for three dimensional shear loading assuming no stretching in the fibers. Energy comparisons with numerical simulations of the material agreed very well with the homogenization results. In this thesis, the same approach will be used to study the instabilities that appear in similar composites under bending. Equation 1.17 will be used to model the matrix and the fibers will be modeled separately in order to be able to distinguish between tension, compression and microbuckling.

Chapter 2

Numerical Simulation

Numerical simulations of the material have been performed in order to evaluate the results of the theoretical model. A finite element model has been created in Abaqus software. The model aims to recreate the micromechanical behavior so it consists of a representative volume element where the fibers and the matrix are modeled separately.

Numerical models have been extensively used to model micromechanics by numerical homogenization in the literature such as in [17]. A Representative Volume Element (RVE) is modeled with periodic boundary conditions and it is assumed that the response is the same as for an infinite solid. These techniques have been used for fiber composites and also for materials with particles ([18]), voids ([19]), two phases, etc.

Since the response of the material under bending is assumed to be periodic throughout the material, only a representative volume element has been simulated. Figure 2.1 shows how the material section is cut. For the numerical simulation, the coordinate system has been defined by aligning the x-axis with the fiber direction and the y-axis with the through-thickness direction. The model is then obtained by cutting the material by two planes parallel to the x-y plane. The process for generating the geometry and the setup of the finite element model are explained in the following sections.

2.1 Model Geometry

A Matlab script has been used for generating the model geometry and the fibers arrangement. The parameters that define the model volume are the thickness t, the width w and the length l. The thickness t and the fibers volume fraction V_f are imposed since they are known properties of the material. The width is initially approximated and it is later readjusted. First, the number of fibers in the cross section that gives the the volume fraction is calculated for the given w. This value (which in general will not be an integer) is then rounded up and the width is recalculated to achieve the desired volume fraction.

The length l of the material is also initially predefined. However, this parameter can affect the results of the numerical simulation. The length of the model will constrain the length that the buckling waves can have. Buckling waves appear in equal divisions of the material length so the maximum half wave length that is allowed is the length of the model itself. Since the strain energy density depends on the buckling wavelength, models with different lengths might get different wavelengths and thus different strain energy densities. The correct wavelength would be obtained from the model with the length that minimizes the strain energy density. In order to compare the results with the theoretical model, the length of the numerical model will be set accordingly to the wave length used in the theoretical model.

Once the model volume has been defined, the distribution of the fibers in the cross section of the material must be determined. The location of the fibers is calculated following the random sequential adsorption algorithm. A detailed explanation of the algorithm is given in [20] and [21]. The fiber arrangements are required to meet certain characteristics. The fibers are randomly placed and if one fiber does not meet the requirements the configuration is discarded and a new one is generated. This random iterative process continues until all the fibers have been located. Figure 2.2 shows some of the fibers arrangements that have been used.

Figure 2.1: Representative volume element.

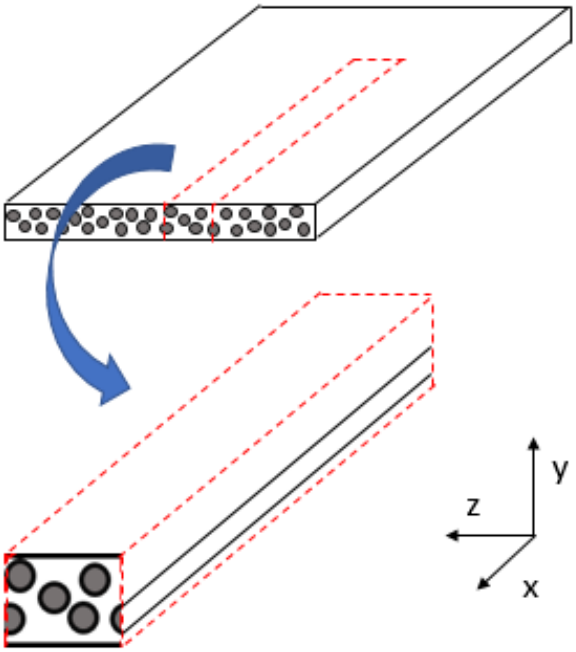

Figure 2.2: Different random fiber arrangements.

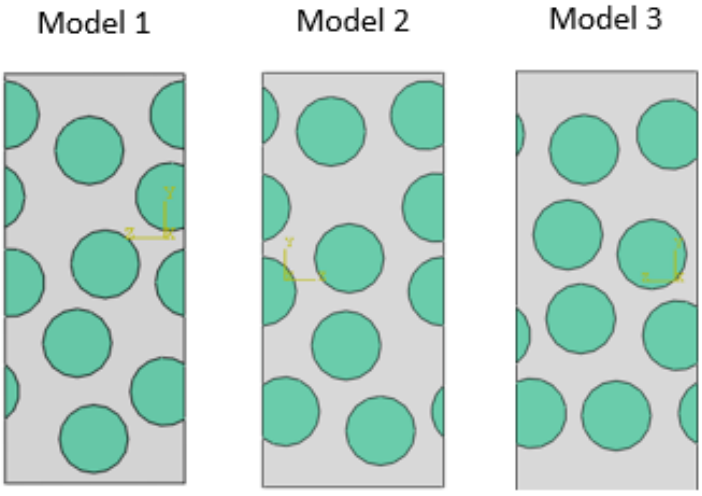

The restrictions in the geometry that have been applied are the following (figure 2.3):

- Fibers are enforced to be separated by a minimum of $0.2r_f$ in order to make easier the meshing of the matrix between the fibers.
- There can not be fiber sections crossing the upper and lower boundaries of the section since those are the boundaries of the laminate. Furthermore, a distance of $0.2r_f$ between the fibers and those borders is again imposed to ensure proper meshing.
- Since the material is assumed to be periodic, if one fiber crosses on boundary of the section the part of the fiber that remains outside the section has to be located on the opposite boundary. Both parts of the fiber need to fulfill the rest of the geometry requirements.
- The centers of the fibers that lay outside the material section have to be within a distance of $0.2r_f$ to the material boundary. If the center was too far from the boundary, the resultant fiber area in the section would be very small and that could cause meshing problems as well.

2.2 Finite element model setup

Once the geometry and the fibers arrangement has been calculated, a parametric model based on the Matlab output is built in Abaqus. The model and the simulation are set up by a Python script that easily allows to change the material parameters by changing the Matlab geometry file. First the model geometry is generated as shown in figure 2.5. Different partitions are created for the matrix and the fibers.

Next, material properties are assigned and then the model is meshed. Both fibers and matrix have been modeled as Neo Hookean and incompressible solids. The elements that have been used for both components are hybrid wedges (Abaqus C3D15H element).

Figure 2.3: Fiber arrangement restrictions

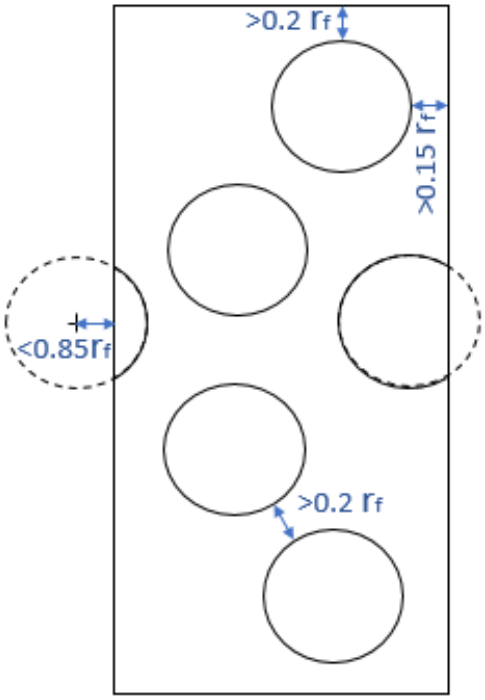

Figure 2.4: Abaqus model.

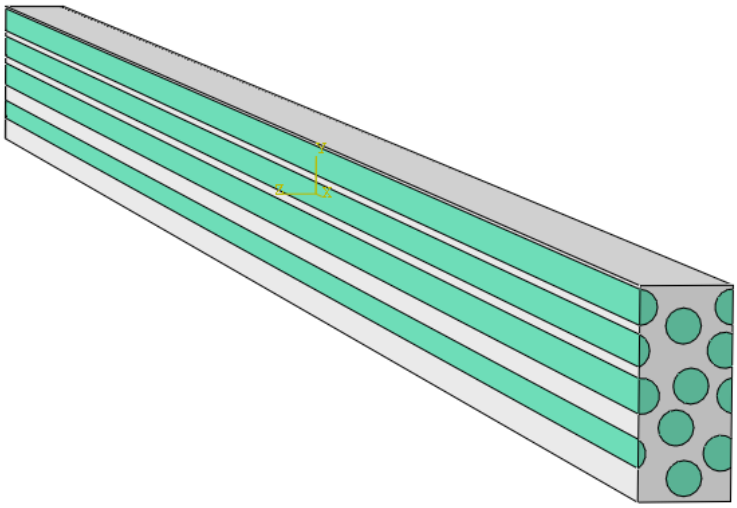

Hybrid elements were needed because of the incompressibility. Other element shapes such as triangular prism could not be tried because the meshes did not allow to apply the periodic boundary conditions. The meshed model is shown in figure 2.5.

Figure 2.5: Abaqus mesh

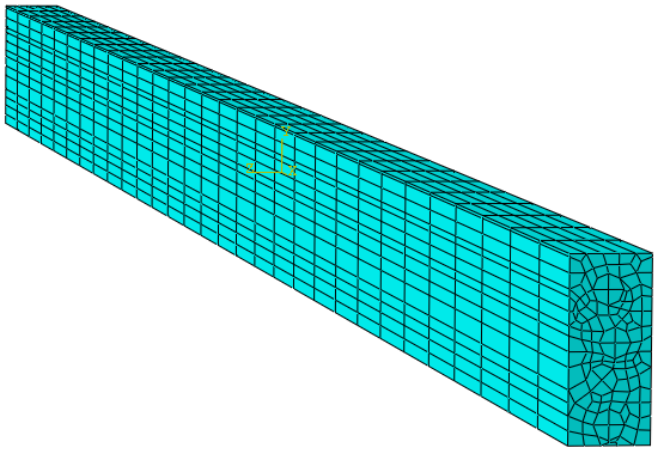

The boundary conditions are periodic in the z direction. They are set node by node in the surfaces that are orthogonal to the z-axis. Each node at the $z = 0$ surface is related to its opposite node at the $z = w$ using the Abaqus 'equation' command. All the displacements are set to be periodic:

$$u_x(x, y, 0) = u_x(x, y, w)$$

$$u_y(x, y, 0) = u_y(x, y, w)$$

$$u_z(x, y, 0) = u_z(x, y, w)$$

The bending is applied by rotating the faces that are perpendicular to the x-axis. The faces are imposed to remain flat by a kinematic copuling. Then a rotation of the same magnitude and opposite sign is applied to each face. The kinematic coupling forces the nodes in the faces to remain in the same plane but they are free to move inside the plane. The rotation is applied through a dummy node for each face. The dummy node is then

connected to the nodes of its corresponding face so that the same rotation is applied to all the nodes. These kinematic constrains are shown in figure 2.6.

Special care had to be taken for the nodes at the borders of the cross section (highlighted in figure 2.6) since they were coupled to the coplanar faces and also linked by periodic boundary conditions to the opposite edge. Every time a constrain is defined in Abaqus a degree of freedom is removed and it can not be used again in another constrain. For this reason, periodic boundary conditions and the face coupling could not be applied directly to the same nodal degree of freedom. A dummy node had to be created for each pair of nodes at the boundaries of the cross section. The face coupling was applied to the dummy node and both nodes at the edges were connected to the dummy node. This relationship was again defined by imposing equal displacements for both nodes with the 'equation' command. As a result, both the face coupling and the periodic conditions could be applied with only one constrain for the nodes at the edges.

Figure 2.6: Boundary conditions: face coupling

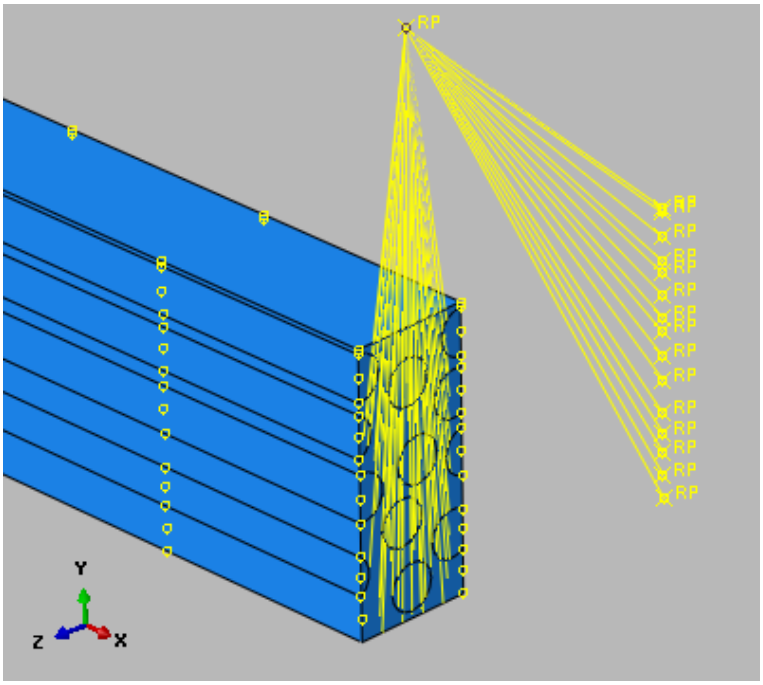

2.3 Analysis results

The obtained deformed configuration is shown in figures 2.7 and 2.8 for a volume fraction of 40%. The results show that the applied bending moment produces constant curvature along the model. Buckling can be observed in the compression. The amplitude of the buckles increases with compression and the wavelength is equal to the model length, which is constrained by the model as was previously explained. Different models with different fiber arrangements and volume fractions showed similar behavior.

Figure 2.7: Deformed configuration in the XY plane

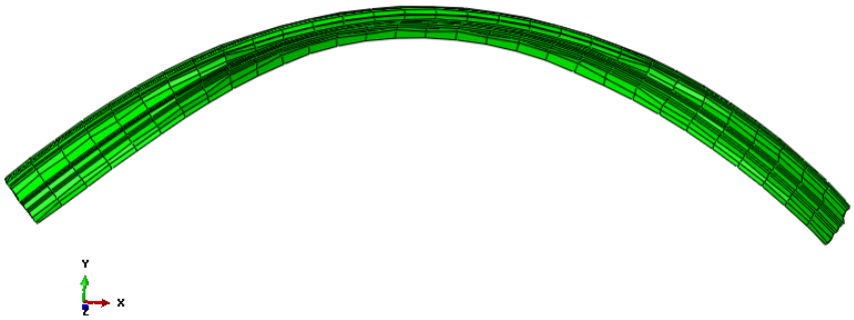

Figure 2.9 shows the Von Misses stress in the cross section at the mid length of the volume. It can be see how the stresses are mostly absorbed by the fibers and how the fibers on the compression side undergo higher displacements and the buckles are more accentuated. The effect of the periodic boundary conditions is also clearly visible. The total strain energy and applied moment are compared with the proposed theoretical model in the following chapter.

Figure 2.8: Deformed configuration in the XZ plane for curvature by thickness $\kappa * t = 0.0935$

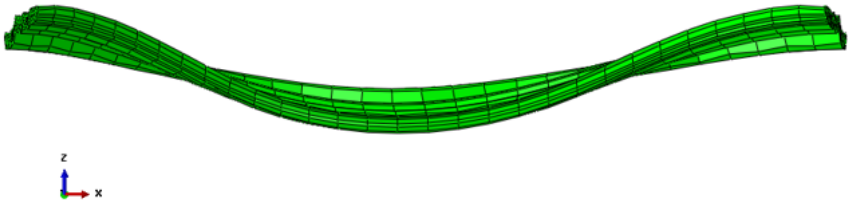

Figure 2.9: Cross section displaying Von Misses stress for curvature by thickness $\kappa * t = 0.0935$

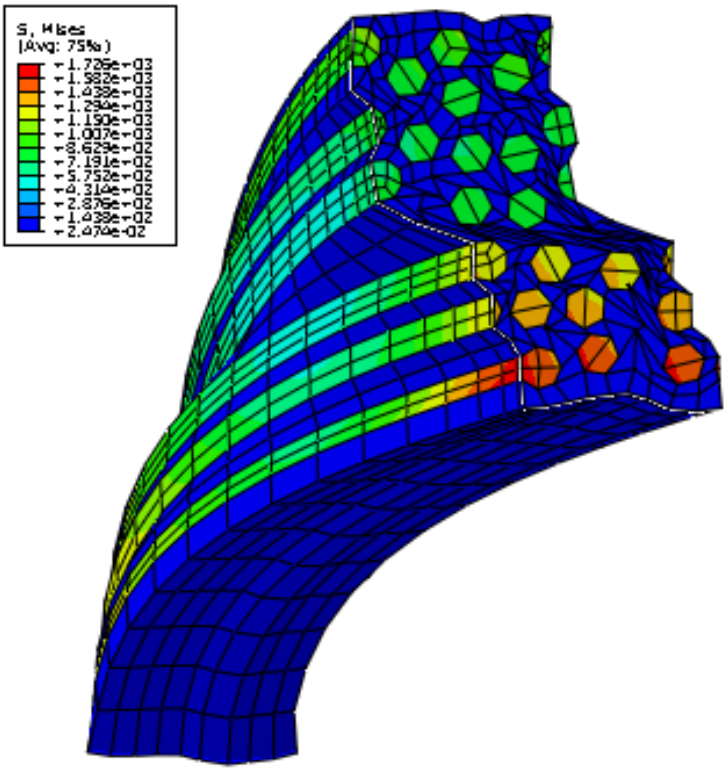

Chapter 3

Theoretical model

In this section, an energy based model is developed in order to predict the mechanical behavior of the composite under bending. The system to be modeled is described in figures 3.1 and 3.2. A micro-mechanical approach is taken, the material is modeled as a hyperelastic Neo Hookean solid and the fiber contributions are included through homogenization methods. Large deformations and incompressibility for the materials are assumed.

Figure 3.1: Laminate under bending. Buckling on the compression side is not seen from this perspective because it is orthogonal to the bending plane.

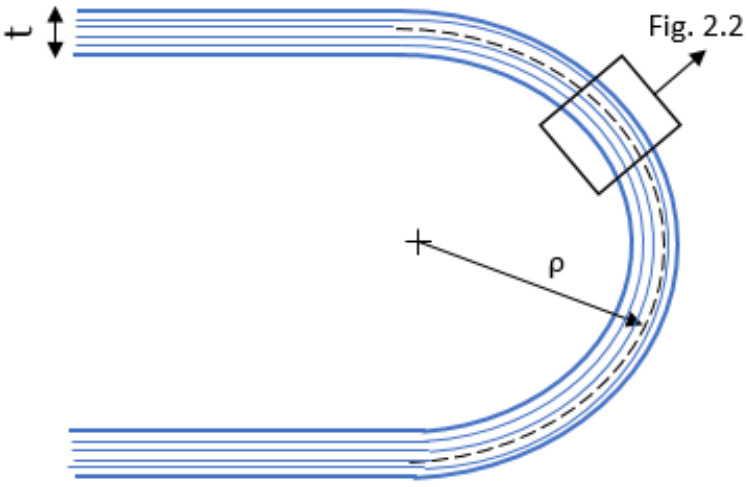

The result is an energy model that is a function of the material geometry and properties

and some unknown kinematic parameters such as the buckling wavelength. These parameters are calculated by minimizing the strain energy as a function of them. However, the strain energy does not have a closed form solution and needs to be integrated numerically. Therefore, a Matlab script has been coded for performing the integration and minimization of the energy.

Figure 3.2: Fraction of the material to be modeled.

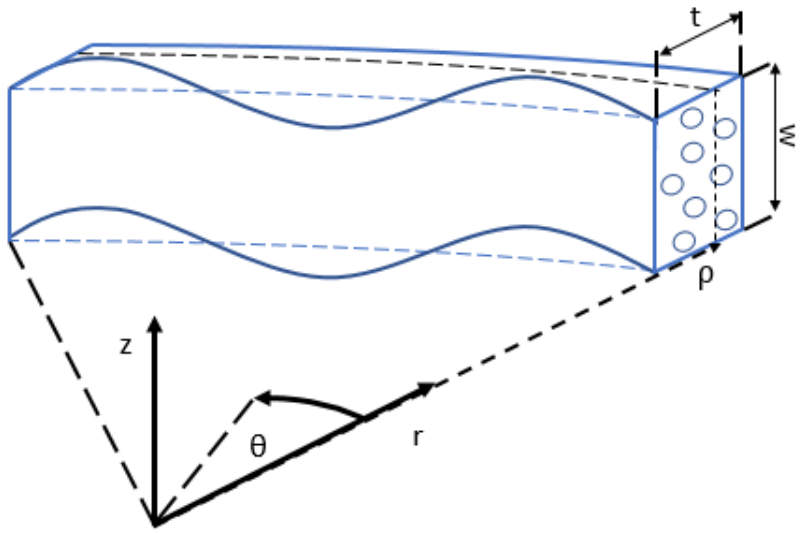

3.1 Kinematics

The kinematic model has been developed based on experimental observations that can be found on the literature ([22] and [1]). Those experiments show that, when this material is subjected to a certain bending, some sinusoidal microbuckling appears on the fibers on the compression side. The buckling seems to be contained in the plane perpendicular to the bending plane. The buckling wave length is assumed to be constant through the thickness with respect to the undeformed configuration. The degree of curvature at which buckling appears and the length of the buckling waves are topics to be addressed in this study.

3.1.1 Displacement field

For simplicity, it has been assumed that the curvature is constant through the whole volume. Therefore, it has been decided to use cylindrical coordinates to represent the deformed material while a Cartesian coordinate system has been chosen for the undeformed reference configuration. The same approach that is described in [23] has been followed to calculate the deformations field. Figure 3.3 shows both coordinate systems in the bending plane. The z coordinate, where the buckling occurs, is perpendicular to that plane and has the same direction in both coordinate systems.

Figure 3.3: Coordinate systems

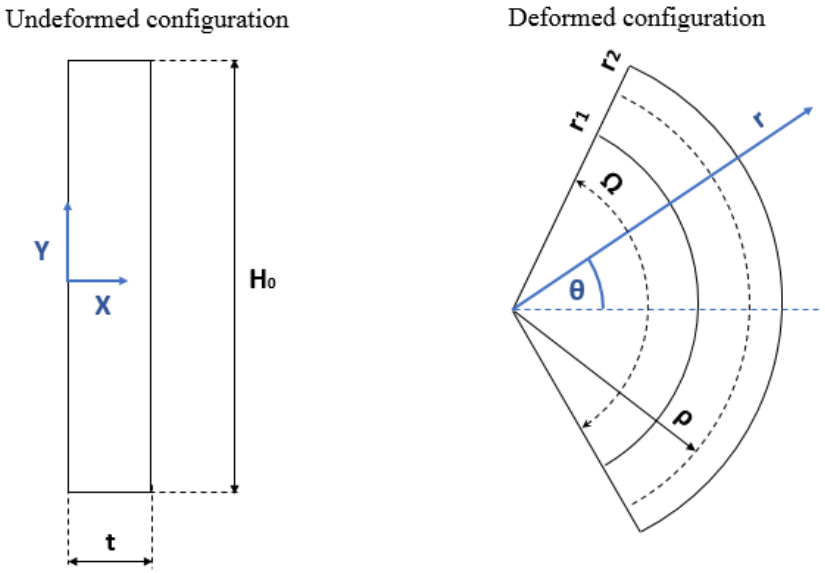

In Figure 3.3, ρ represents the position of the neutral surface, where the stress is zero and thus the length does not change. This implies that the following relation is always maintained:

$$\rho\ \Omega = H_0 \tag{3.1}$$

And the bending curvature is defined as:

$$\kappa = \frac{1}{\rho} \tag{3.2}$$

Notice also that the thickness is free to change. So the difference between r_1 and r_2 will not coincide with the initial thickness. These values will be determined by assuming that the material is incompressible. Furthermore, the relative position of r_1 and r_2 to the neutral surface is not known either. This will be one of the variables found by minimizing the total strain energy.

The microbuckling is produced along the axial direction and remains perpendicular to the bending plane. So displacements take a sinusoidal shape in the z-axis and follow along the θ direction. This phenomenon does not necessarily appear in all the compressed region. The most compressed fibers will be the first to buckle but the ones close to the neutral surface might remain straight. The function that determines when and where buckling is produced will be also obtained from the energy minimization.

Once all this factors are taken into account, the deformed configuration can be formulated as a function of the original coordinates :

$$r = f(X) \tag{3.3}$$

$$\theta = \frac{Y}{\rho} \tag{3.4}$$

$$z = Z + a \sin\left(\frac{\pi}{L_0} Y\right) \qquad for\ the\ buckled\ regions \tag{3.5}$$

$$z = Z \qquad for\ the\ non\ buckled\ regions \tag{3.6}$$

where $f(X)$ is the function that determines the relationship of the radial coordinates and its position at the undeformed reference system. This function will be defined later.

According to figure 3.3 r,θ and z will refer to the deformed configuration coordinate system and X,Y and Z to the undeformed coordinate system. a and L_0 stand for the buckling amplitude and the wavelength with respect to the undeformed configuration. Note that L_0 is the undeformed arclength of the fiber in half period of the buckle and it is constant through X. However, it is not the real wavelength of the deformed fibers which can be directly related to the buckling amplitude. The relationships between all these parameters and the fibers strains will be explained in the following section.

The function for the radial coordinate $f(x)$, which will determine the limits r_1 and r_2, can now be obtained by assuming that the material is incompressible. This implies that the determinant of the deformation gradient tensor is equal to one.

For the chosen coordinate systems:

$$F_{Xr} = \begin{bmatrix} \frac{dr}{dX} & \frac{dr}{dY} & \frac{dr}{dZ} \\ r\frac{d\theta}{dX} & r\frac{d\theta}{dY} & r\frac{d\theta}{dZ} \\ \frac{dz}{dX} & \frac{dz}{dY} & \frac{dz}{dZ} \end{bmatrix} \tag{3.7}$$

By introducing the displacement field all the components of the tensor are obtained:

$$\frac{dr}{dX} = \frac{df}{dX} \quad ; \quad \frac{dr}{dY} = 0 \quad ; \quad \frac{dr}{dZ} = 0 \tag{3.8}$$

$$\frac{d\theta}{dX} = 0 \quad ; \quad \frac{d\theta}{dY} = \frac{1}{\rho} \quad ; \quad \frac{d\theta}{dZ} = 0 \tag{3.9}$$

$$\frac{dz}{dX} = \frac{da}{dX}\sin\left(\frac{\pi}{L_0}Y\right) \tag{3.10}$$

$$\frac{dz}{dY} = a\cos\left(\frac{\pi}{L_0}Y\right)\frac{\pi}{L_0} \tag{3.11}$$

$$\frac{dz}{dZ} = 1 \tag{3.12}$$

$$F = \begin{bmatrix} \frac{dr}{dX} & 0 & 0 \\ 0 & r\frac{d\theta}{dY} & 0 \\ \frac{dz}{dX} & \frac{dz}{dY} & \frac{dz}{dZ} \end{bmatrix} \tag{3.13}$$

Setting $detF = 1$ it is obtained that:

$$\left(\frac{dr}{dX}\right)\left(\frac{r}{\rho}\right) = 1 \quad \rightarrow \quad r = \sqrt{2\rho X + \beta} \tag{3.14}$$

By substituting $X = 0$ in the function $r(X)$, we find that $\beta = r_1^2$. This term is related to the change in the thickness of the material and the relative position of the neutral surface. It can not be determined by the assumptions made for this model so it will be treated as a variable to minimize the strain energy.

3.1.2 Buckling amplitude and wavelength

In order to establish a relationship between the initial length and the longitudinal strains it is necessary to introduce to different strain functions. The variation in the length of the fibers is assumed to be affected by two different mechanisms. The first are the compression and and tension that appear in a pure bending problem. This will be quantified with λ_c.

For the regions where there is no buckling, this parameter is easily defined since it is just the stretching due to the bending (Figure 3.4):

$$H_0\lambda_c = H \tag{3.15}$$

Where H_0 is the original length of the material and $H(X)$ is a function that represents the length of the deformed material that varies along the thickness. λ_c can be obtained geometrically just by using the fact that the length at the neutral surface remains constant, so it is equal to H_0. Then this relation is used to calculate the new length at the deformed areas.

$$H_0 = \rho\ \Omega \tag{3.16}$$

$$H(X) = r(X)\ \Omega \tag{3.17}$$

Eliminating Ω:

$$\lambda_c = \frac{H(X)}{H_0} = \frac{r(X)}{\rho} \tag{3.18}$$

This is enough to describe the strains on the areas where there is no buckling. For the other regions, the contribution of buckling will be included through the parameter λ_b. This will complicate the definition of the strains and add more variables that are not predetermined to our problem. These include the buckling wavelength and the function that defines the presence of buckling throughout the thickness.

Figure 3.4: Radial and thickness geometric relationships

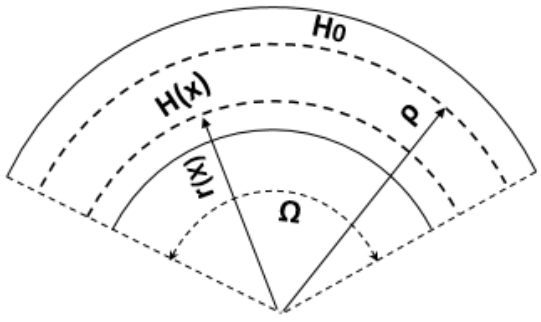

In order to simplify the processes and reduce as much as possible the number of variables to be calculated by numerical optimization, the following constraints are added:

- The fibers can be compressed while they are buckling. A new functionn λ_{cb} needs to be introduced since the compression deformation is no longer λ_c as was previously defined. The function λ_{cb} is unknown and it will be obtained by relating it to λ_b, which is also an unknown.

- The parameter L_0 is set to be constant in X. This implies that the wavelength mapped on the undeformed configuration is constant through the thickness and that the parameter L, which is the wavelength in the deformed volume, varies linearly and proportionally to λ_c as shown in figure 3.5:

$$L_0\lambda_c(X) = L(X) \tag{3.19}$$

  This assumption actually agrees with the experimental observations.

- L_0 is considered only to be a function of the materials and geometry properties and it is not influenced by curvature. The value will be obtained as the wavelength that minimizes the energy density. For a certain degree of curvature, the strain energy will start to be lower if buckling appears. At that point, L_0 will take the value that minimizes the energy and will remain constant for higher curvatures.

Where microbuckling is present, λ_b determines the relationship between the buckling wavelength $L(X)$ and the actual total length of the buckled fibers. At the regions where there is no buckling, λ_b is simply equal to one. The relationship is given by:

$$L_0\lambda_{cb}(X)\lambda_b(X) = L_f(X)\lambda_b(X) = L(X) \tag{3.20}$$

And λ_c can now be expressed as:

$$\lambda_c = \lambda_{cb}\lambda_b \tag{3.21}$$

Figure 3.5: Geometric relationship between $L0$ and L.

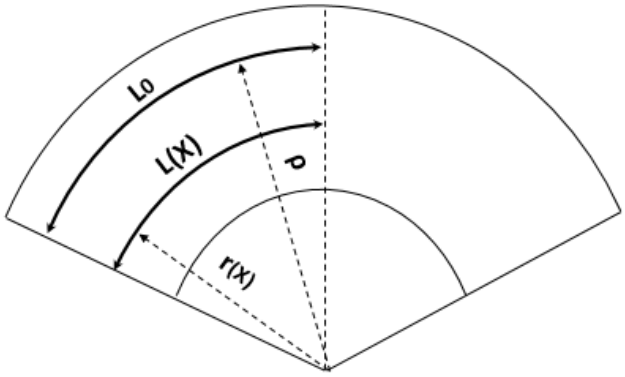

Figure 3.6: Pre and postbuckling fiber deformations.

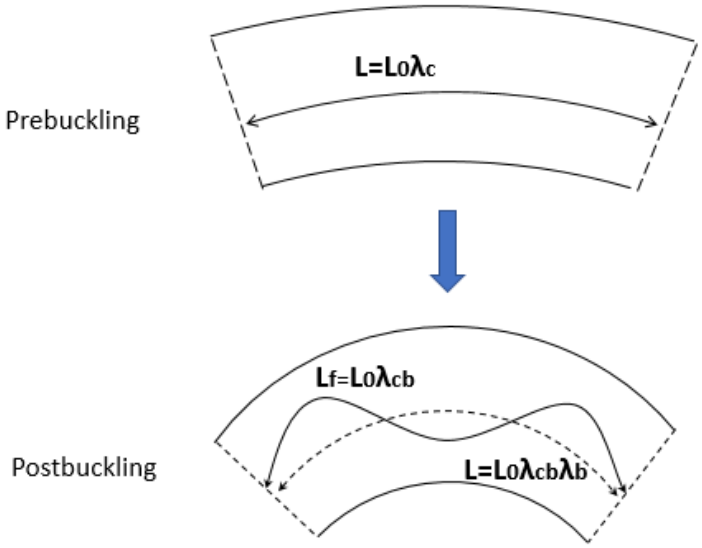

Where L_f denotes the total length of the buckled fibers after taking into account the compression strains (figure 3.6). This value might change as the curvature increases and will affect the amplitude of the buckling. The higher the compression strains, the lower the buckling amplitude will be.

Note that λ_b is a function of X, hence it varies through the thickness. It will take the value of one in the areas where there is no buckling and will be higher than 1 if there is buckling. The buckling is expected to be higher where the compression is higher but it might not appear in the whole compressed side. The buckling function will be obtained by minimizing the strain energy. The relationship between λ_{cb} and λ_b will be used to reduce the number of unknowns to be find in the minimization:

$$\lambda_{cb} = \frac{L(X)}{L_0 \lambda_b} = \frac{r(X)}{\rho \lambda_b} \tag{3.22}$$

Figure 3.7: Buckling amplitude and wavelength relation

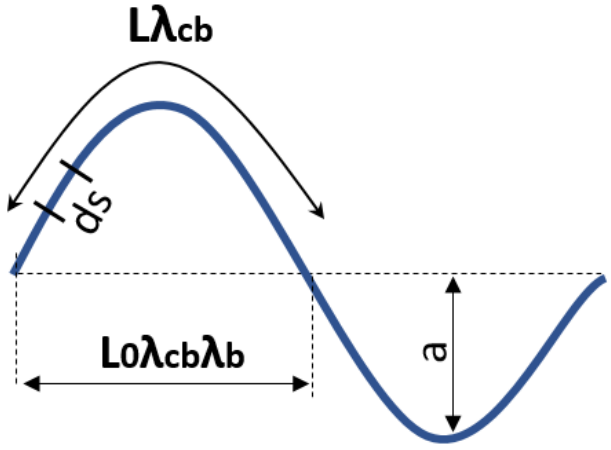

Now the only kinematic parameter left to be defined is the buckling amplitude a. This term is also calculated by assuming that buckled fibers are incompressible. This implies that

the effect of λ_b is neglected but this should only produce a very small error and simplifies significantly the calculation. Following the approach from [1], the total length of the fibers is integrated as the arclength of a sinusoidal function as figure 3.7 shows.

$$L_f = \int_0^{L_f} ds = \int_0^{L(X)} \sqrt{1 + \left[\frac{\pi a}{\lambda}\cos\left(\frac{\pi y}{L}\right)\right]} dy \tag{3.23}$$

This integral is a complete elliptic integral of the second kind. It does not have a closed form solution but can be expressed in numerical series.

$$L_f = \frac{2\mathrm{L}(X)}{\pi} EllipticE\left[\left(\frac{a\pi}{L(X)}\right)^2\right] \tag{3.24}$$

Since $L = L_f\lambda_b$, the relationship between the amplitude and the wavelength can be nondimensionalized:

$$\frac{L_f}{L} = \frac{1}{\lambda_b} = \frac{2}{\pi} EllipticE\left[\left(\frac{a\pi}{\lambda}\right)^2\right] \tag{3.25}$$

This gives another equation that will be used in the minimization process to remove one more unknown function, the amplitude, which will be set as a function of λ_b.

3.2 Energy model

Once all the kinematic relations have been established we are ready to formulate the energy model. The total energy is modeled as the sum of the contributions of the matrix and the fibers.

$$W = W_m + W_f \tag{3.26}$$

The matrix is modeled as an incompressible Neo Hookean solid. From the nonlinear homogenization theory, we recover the expression for the energy of a fiber-reinforced Neo Hookean solid. It is assumed that fibers do not stretch to simplify the solution. The stretching of the fibers due to the bending is actually very small so this assumption should not

cause a significative error. According to [16], the expression fort this case reads:

$$W_m = W_{IH}(I_4 = 1) = \frac{\mu_{IH}}{2}(I_1 - 3) - \frac{\mu_{IH} - \mu_{HS}}{2}(I_5 - 1) \tag{3.27}$$

Where μ_{IH} and μ_{HS} were derived in Section 1.3.2 using homogenization.

$$\mu_{ih} = (1 - V_f)^2 \left(1 + \frac{2(2 - V_f)V_f}{(1 - V_f)^2}\frac{\mu_f}{mu_m} + \frac{\mu_f^2}{\mu_m^2}\right)\frac{\mu_m}{2} - (1 - V_f)^2\frac{\mu_f - \mu_m}{2}$$

$$\times\sqrt{\frac{2}{(1 - V_f}})^2\frac{\mu_f}{\mu_m} + \left(1 + \frac{2(2 - V_f)V_f}{(1 - V_f)^2}\frac{\mu_f}{mu_m} + \frac{\mu_f^2}{\mu_m^2}\right) \tag{3.28}$$

$$\mu_{hs} = \frac{(1 - V_f)\mu_m + (1 + V_f)\mu_f}{(1 + V_f)\mu_m + (1 - V_f)\mu_f}\mu_m \tag{3.29}$$

The first term of the equation for W_{IH} coincides with the expression of the energy of a Neo Hookean solid, which in this case will correspond to the matrix energy. The term that contains I_5 adds significant complexity to the problem and adds too many numerical terms to the equation. Therefore, as a first approach to the problem it will be neglected.

The proposed homogenization method is not capable of representing the microbuckling. Hence, the fibers will be modeled separately using beam theory. The following sections describe the derivation of the energy of the fibers and the matrix for both the pre-buckling and post-buckling regimes.

3.2.1 Strain Energy of the matrix

The matrix is considered as a hyperelastic incompressible material. Ignoring the fibers for now and considering a homogeneous material, its energy is modeled as:

$$W_m = \frac{\mu_m}{2}(I_1 - 3) \tag{3.30}$$

Where μ_m is the matrix shear modulus and I_1 is the first invariant of the Cauchy-Green deformation tensor.

$$I_1 = tr(C) \tag{3.31}$$

And the Cauchy-Green tensor is calculated with the deformation gradient that was already obtained in the previous section:

$$C = F^T F \tag{3.32}$$

$$C = \begin{bmatrix} \left(\frac{dr}{dX}\right)^2 + \left(\frac{dz}{dX}\right)^2 & \frac{dz}{dX}\frac{dz}{dY} & \frac{dz}{dX}\frac{dz}{dZ} \\ \frac{dz}{dX}\frac{dz}{dY} & r^2\left(\frac{d\theta}{dY}\right)^2 + \left(\frac{dz}{dY}\right)^2 & \frac{dz}{dY}\frac{dz}{dZ} \\ \frac{dz}{dX}\frac{dz}{dZ} & \frac{dz}{dY}\frac{dz}{dZ} & \left(\frac{dz}{dZ}\right)^2 \end{bmatrix} \tag{3.33}$$

After eliminating the terms that were zero. The trace reads as:

$$I_1 = tr(C) = \left(\frac{dr}{dX}\right)^2 + \left(\frac{dz}{dX}\right)^2 + r^2\left(\frac{d\theta}{dY}\right)^2 + \left(\frac{dz}{dY}\right)^2 + \left(\frac{dz}{dZ}\right)^2 \tag{3.34}$$

Finally, the total strain energy contained in the material is obtained by integrating the energy density W_m in the total volume.

$$\overline{W}_m = \int_V \frac{\mu_m}{2}(I_1 - 3)dV \tag{3.35}$$

Neo Hookean energy model without buckling

First the energy is going to be calculated for the regions that do not buckle. For this simple case of an homogeneous material without buckling, the deformation gradient components involved take the following values:

$$\frac{dr}{dX} = \frac{\rho^2}{2\rho X + \beta} \quad ; \qquad \frac{d\theta}{dY} = \frac{r}{\rho} \tag{3.36}$$

$$\frac{dz}{dX} = 0 \qquad \frac{dz}{dY} = 0 \qquad \frac{dz}{dZ} = 1 \tag{3.37}$$

Substituting this values in the energy equation we get an integral that has a closed form solution.

$$\overline{W}_{mnb} = \int_V \frac{\mu}{2}\left(\frac{\rho^2}{2\rho X+\beta} + \frac{2\rho X+\beta}{\rho^2} - 2\right) dV = \frac{\mu}{2} wl \left[\frac{\rho}{2} ln(2\rho X+\beta) + \frac{X^2}{\rho} + \left(\frac{\beta - 2\rho^2}{\rho^2}\right) X\right]_0^t =$$

$$= \frac{\mu}{2} hl \left(\frac{\rho}{2} ln(\frac{2\rho t+\beta}{\beta}) + \frac{t^2}{\rho} + \left(\frac{\beta - 2\rho^2}{\rho^2}\right) t\right) \tag{3.38}$$

The parameter β is related to the position of the neutral axis as it was already explained. It is calculated by minimizing the energy. For this case it has the following closed form solution.

$$\frac{d\overline{W}}{d\beta} = 0 \rightarrow \beta = \rho(\sqrt{t^2+\rho^2} - t) \tag{3.39}$$

Figure 3.8: Deformed Abaqus model for a homogeneous material.

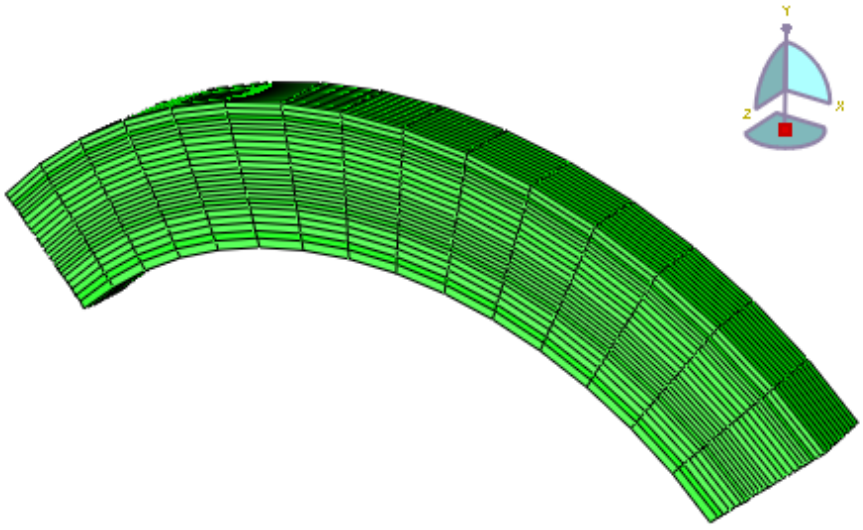

In order to validate this solution, it has been compared with the beam theory results and a numerical simulation. The numerical simulation uses the same Abaqus model that has been used for the buckling calculations, the only difference is that in this case the material is homogeneous. The results are shown in figure 3.8. For the beam, it has been assumed that it is a plain strain case since strain remain on the bending plane. The according expression for the strain energy is:

$$\overline{W}_{beam} = \frac{1}{2}\frac{EI}{1-\nu^2}\kappa^2 l \tag{3.40}$$

Figure 3.9: Strain Energy for length/thickness=6.

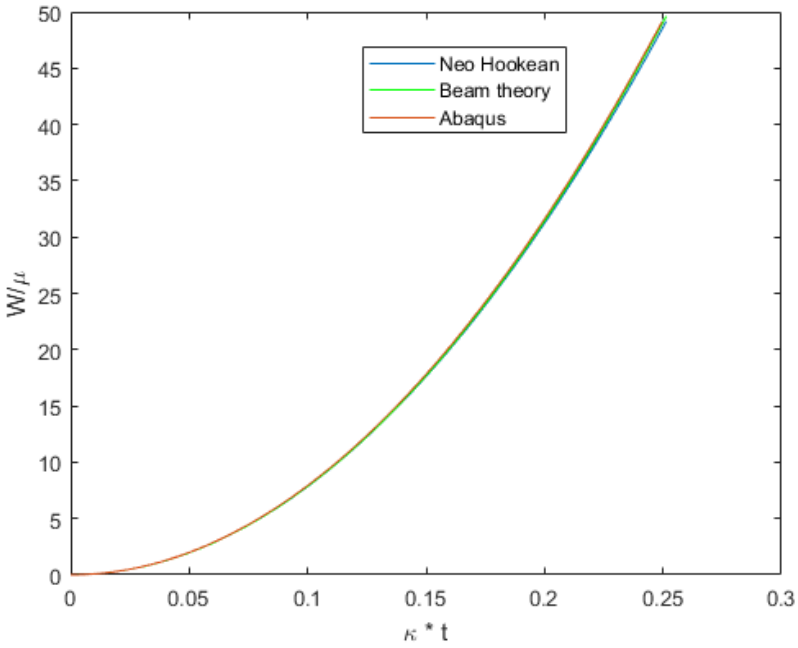

The results show perfect agreement between the three methods for a slender beam (figure 3.9). Since the beam theory does not work for thick beams, when the length/thickness ratio is increased it starts to differ from the Neo Hookean and the Abaqus model as shown in figure 3.10.

Figure 3.11 shows the coordinates of r_1, r_2 and ρ. This shows that the obtained value

of β is in agreement with the geometry of the problem. r_1 and r_2 are functions of *beta* and it can be seen that ρ falls between these two parameters for all the curvatures, otherwise the value of β would be incorrect. Furthermore, the figure also shows that ρ is approximately on the middle of the section as expected for the Neo Hookean model for small strains.

Neo Hookean energy model with buckling

This case adds to the previous case two terms in the expression of I_1. These can not be analytically integrated in the volume because of the amplitude a and its derivative do not have closed form solutions so a numerical approach will be used.

$$\frac{dz}{dX} = \frac{da}{dX}\sin\left(\frac{\pi}{L}Y\right) \tag{3.41}$$

$$\frac{dz}{dY} = a\cos\left(\frac{\pi}{\lambda}Y\right)\frac{\pi}{L} \tag{3.42}$$

Therefore, the strain energy has been divided into W_a and W_n for convenience. W_a is the part of the integral that has a closed form solution and is independent of the buckling. It actually coincides with the solution for the case where buckling is not considered. W_n must be integrated numerically and includes only the terms that involve buckling so it becomes zero at the regions without buckling. The total strain energy of the material is then calculated as:

$$\overline{W}_{mb} = \overline{W}_a + \overline{W}_n \tag{3.43}$$

$$\overline{W}_a = \int_V \frac{\mu}{2}\left(\left(\frac{dr}{dX}\right)^2 + r^2\left(\frac{d\theta}{dY}\right)^2 + \left(\frac{dz}{dZ}\right)^2 - 3\right)dV \tag{3.44}$$

$$\overline{W}_a = lw\frac{\mu}{2}\left(\frac{\rho}{2}\ln\left(\frac{2\rho t+\beta}{\beta}\right) + \frac{t^2}{\rho} + \left(\frac{\beta-2\rho^2}{\rho^2}\right)t\right) \tag{3.45}$$

$$\overline{W}_n = \int_V \frac{\mu}{2}\left(\left(\frac{dz}{dX}\right)^2 + \left(\frac{dz}{dY}\right)^2\right)dV \tag{3.46}$$

Figure 3.10: Strain Energy for length/thickness=2.

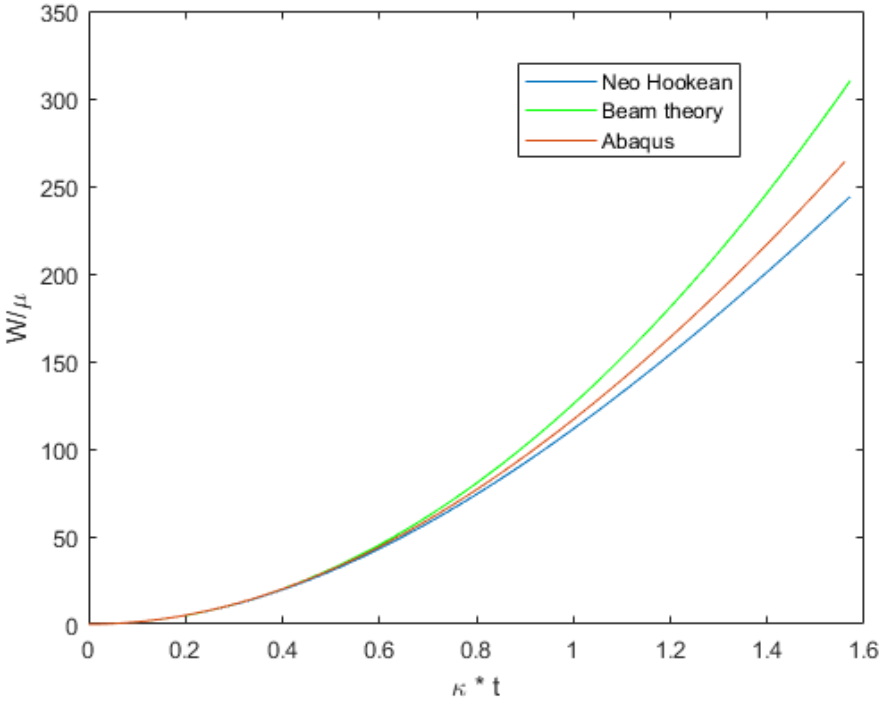

Figure 3.11: Positions of ρ,r_1 and r_2 as a function of curvature.

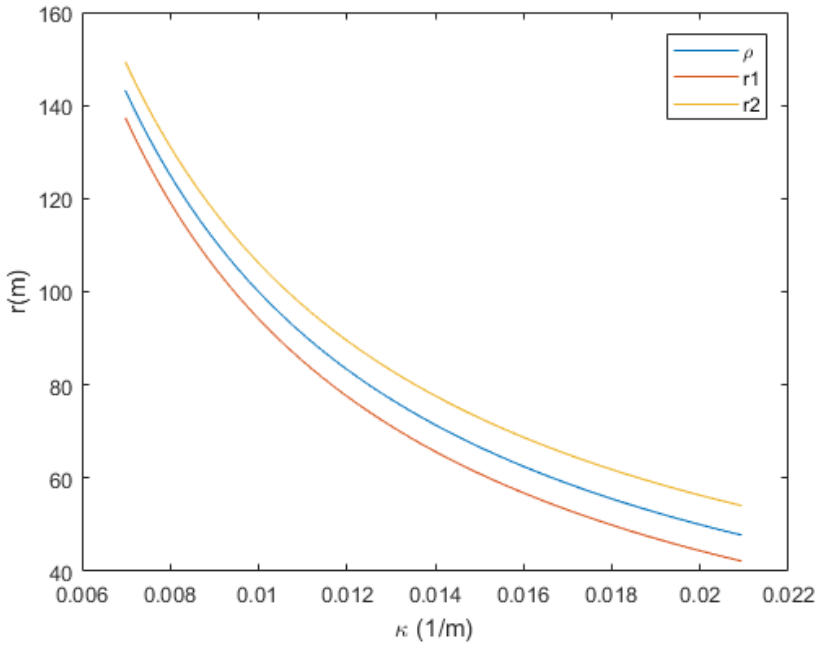

After integrating on Y and Z, W_n becomes

$$\overline{W}_n = \frac{\mu}{2} w \int_0^t \left[\left(\frac{da}{dX} \right)^2 \frac{l}{2} + \left(\frac{a\pi}{\text{Ł}(X)} \right)^2 \frac{l}{2} \right] dX \tag{3.47}$$

which needs to be integrated numerically because a and λ do not have a closed form solution. The trapezoidal integration rule has been used to compute this integral. The derivative of the amplitude is numerically approximated as well.

The strain energy is then minimized in order to find the values of β and λ_b which are unknown. This is achieved by using the Matlab function *fmincon*. This solver numerically minimizes a function for some input variables that have certain constrains. The input variables are estimated values for β and $\lambda_b(X)$, which is introduced as a vector whose components are the values of the function discretized through the thickness. For this case, the constrains are the kinematic relationships:

- The limits of β are given by the constrains on the neutral axis, which has to remain inside the material volume limits. In the case that ρ coincides with r_1, we get that

$$\beta < r_1^2 \tag{3.48}$$

  For the upper limit, if ρ is equal to r_2

$$\beta > r_2^2 - 2\rho t \tag{3.49}$$

- The buckling deformation function λ_b is just limited by the fact that it always compresses the material so it has to be equal or less than one:

$$\lambda_b \leq 1 \tag{3.50}$$

3.2.2 Strain Energy of the fibers

The fibers are modeled based on beam theory. The Strain Energy of the fibers is divided in two terms: the energy due to the compression and the traction of the fibers and the energy due to the buckling.

$$W_f = W_{fc} + W_{fb} \tag{3.51}$$

The strain energy due to compression for one fiber is simply defined as the energy of a beam with axial compression:

$$W_{fc} = \frac{1}{2}E_f\epsilon^2 A_f l = \frac{1}{2}E_f(1-\lambda_c)^2 A_f l = \frac{1}{2}E_f(1-\lambda_c)^2 A_f l \tag{3.52}$$

Where l is the length of the fiber. The other component of the energy is given by the strains caused by the buckling. This term is defined as the classic strain energy of a beam under bending:

$$dW_{fb} = \frac{1}{2}E_f I_f \left(\frac{d^2Z}{dY^2}\right)^2 dY = \frac{1}{2}E_f I_f \left(a\left(\frac{\pi}{L_0}\right)^2 sin\left(\frac{\pi}{L_0}Y\right)\right)^2 dY \tag{3.53}$$

Integrating for one fiber along its axial direction:

$$W_{fb} = \int_0^l dW_{fb} = \frac{1}{4}E_f I_f \left(a\frac{\pi^2}{L_0^2}\right)^2 l \tag{3.54}$$

In order to compute the energy of the percentage of fibers present in the material volume, the energy of one fiber is divided by its cross sectional area to get the area energy density. Then it is integrated in the cross section area of the material and multiplied by the volume fraction.

$$\overline{W}_{fb} = V_f l w \int_0^t \left(\frac{1}{2}E_f(1-\lambda_{bc})^2 + \frac{1}{4}E_f\frac{I_f}{A_f}\left(\frac{a\pi^2}{L_0^2}\right)^2\right) dX \tag{3.55}$$

This component of the energy also needs to be integrated numerically because of the numerical functions present in the integral. Note that λ_c has been substituted by λ_{bc} when

buckling has been added. In the numerical scheme it is calculated as a function of λ_b, so the integral becomes:

$$\overline{W}_{fb} = V_f l w \int_0^t \left(\frac{1}{2} E_f (1 - \frac{r(X)}{\rho \lambda_b(X)})^2 + \frac{1}{4} E_f \frac{I_f}{A_f} \left(\frac{a\pi^2}{L_0^2} \right)^2 \right) dX \tag{3.56}$$

So the unknown variables that need to be found in the minimization are the same that the ones found in the expression for the matrix energy.

3.2.3 Strain Energy of the composite

Strain energy of the composite without buckling

The energy of the model including the fibers is first calculated without buckling. This will serve to validate the buckling model at low curvatures before buckling appears. At this stage, both models should give the exact same result. They will start to differ when buckling appears so this model will be helpful to determine when that happens.

For this case, the energy of the fibers is only due to the tension and compression strains. Since the buckling function is also zero, the volume integral of the axial strains has a closed form solution:

$$\overline{W_f} = \overline{W}_c = \frac{1}{2} V_f w E_f l \left((r_2 - r_1) + \frac{r_2^3 - r_1^3}{3\rho^2} - \frac{l}{\rho}(r_2^2 - r_1^2) \right) \tag{3.57}$$

Where : $r_1 = \sqrt{\beta}$ and $r_2 = \sqrt{2\rho t + \beta}$

The total energy is calculated as the sum of the Neo Hookean model and the fibers contribution.

$$\overline{W} = \overline{W}_c + \overline{W}_{mnb} =$$
$$= \frac{1}{2} V_f w E_f l \left((r_2 - r_1) + \frac{r_2^3 - r_1^3}{3\rho^2} - \frac{l}{\rho}(r_2^2 - r_1^2) \right) + \frac{\widetilde{\mu}}{2} h l \left(\frac{\rho}{2} ln(\frac{2\rho t + \beta}{\beta}) + \frac{t^2}{\rho} + \left(\frac{\beta - 2\rho^2}{\rho^2} \right) t \right) \tag{3.58}$$

As on he previous cases, β needs to be obtained by minimization. For this equation there is no closed form solution so it has been minimized numerically.

Strain energy of the composite with buckling

The total strain energy when buckling is included is obtained as the sum of the matrix buckling model and the fibers:

$$\overline{W} = \overline{W}_{mb} + \overline{W}_{fb} \tag{3.59}$$

Substituting the terms, the complete expression becomes:

$$\overline{W} = lw\frac{\mu}{2}\left(\frac{\rho}{2}\ln\left(\frac{2\rho t+\beta}{\beta}\right)+\frac{t^2}{\rho}+\left(\frac{\beta-2\rho^2}{\rho^2}\right)t\right)+\frac{\mu}{4}wl\int_0^t\left[\left(\frac{da}{dX}\right)^2+\left(\frac{a\pi}{L_0}\right)^2\right]dX+$$

$$V_f lw\int_0^t\left(\frac{1}{2}E_f\left(1-\frac{r(X)}{\rho\lambda_b(X)}\right)^2+\frac{1}{4}E_f\frac{I_f}{A_f}\left(\frac{a\pi^2}{L_0^2}\right)^2\right)dX \tag{3.60}$$

The integrals that contain buckling terms are numerically integrated as explained before. Then the total strain energy is minimized with the same method that was explained for the previous buckling cases.

3.3 Results

In this section, the strain energy and the applied moment obtained in the theoretical model are compared with the results from the numerical simulations described in Section 2. For this comparison, the geometry has been defined relatively to the radius of the fiber: $l = 300r_f$, $t = 18r_f$ and $w = 9r_f$. The shear strain relationship between the fibers and the matrix has been set to $\frac{\mu_f}{\mu_m} = 100000$. All these ratios are representative for soft matrix composites.

Figure 3.12 shows the strain energy results. For the pre buckling regime, the results from the numerical simulations agree quite well with the theoretical model that does not include microbuckling in the fibers. The curvature at which buckling was first observed in the numerical simulations coincides with the drop in the energy of models 1 and 2 in the figure. That behavior is not that clear for model 3, however, in the numerical simulation

buckling appeared around $0.012\kappa * t$. Therefore, the transition to buckling can be in general identified by a deviation of the energy with respect to the no-buckling model.

The theoretical model that includes buckling separates from the no-buckling model at a very low curvature. This result differs significantly from the behavior observed at the numerical simulations. Hence, the buckling model fails to predict the strain energy in the microbuckling regime and when microbuckling appears .

The following figures show the results for different volume fractions. The comparison in figure3.14 shows the same result as on the previous cases: the analytical model predicts that buckling appears before it does in the numerical simulations and therefore the energy is significantly lower.

The numerical results for a volume fraction of 20% and 40% show that buckling appears first for a lower volume fraction. The plots do not show clearly where buckling appeared for the 30% volume fraction. However, in the graphical results from the numerical simulation buckling appeared around $\kappa * t = 14$, which lays in between the other two cases. Therefore, it was confirmed that buckling appears before for lower volume fractions.

Figure 3.15 shows the energy and moment per width only in the matrix for the same cases. This are the results from the numerical simulations. The energy is several orders lower than in the whole material and it only becomes significant when buckling appears. This coincides with the sudden increase of the energy on each of the functions.

The influence of the fiber/matrix shear modulus ratio was also studied. It was found that for ratios lower than approximately $\mu_f/\mu_m = 1000$ buckling does not appear. Figure 3.16 shows the comparison between different ratios for a $V_f = 40\%$.

Finally, the results where compared with the model proposed in [1]. The comparison has been made for $V_f = 40\%$ and $\mu_f/\mu_m = 100000$. The main difference between the two models is that Francis' model does not include the pre-buckling stage. For the post-buckling regime, (after $\kappa * t = 0.034$), Francis' model clearly overestimates the energy while the proposed model is too low compared to the numerical results.

Figure 3.12: Normalized strain energy from theoretical results and numerical simulations.

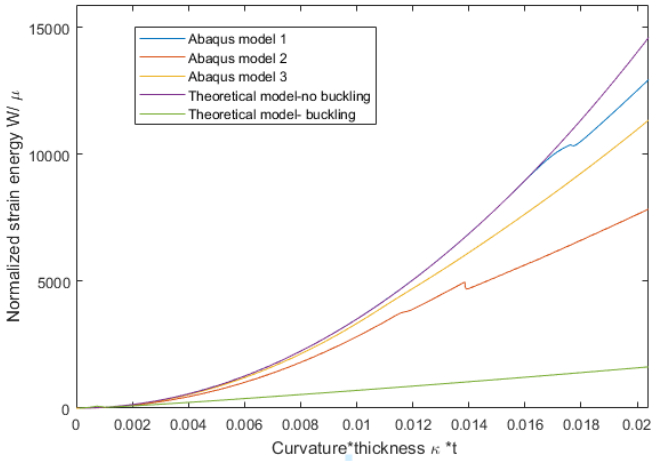

Figure 3.13: Moment per width from theoretical results and numerical simulations.

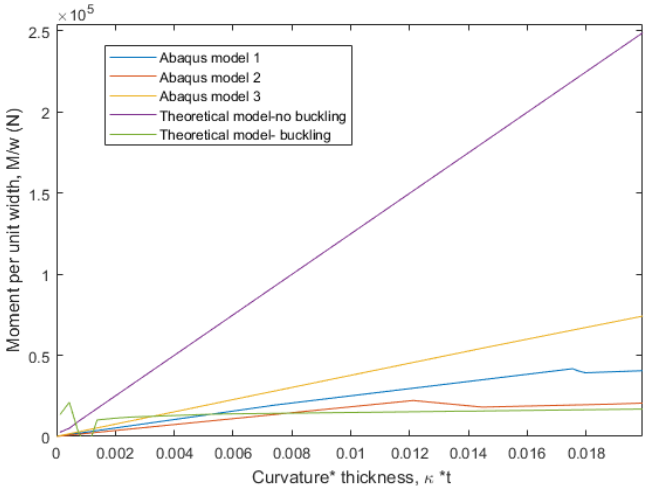

Figure 3.14: Strain energy for different volume fractions.

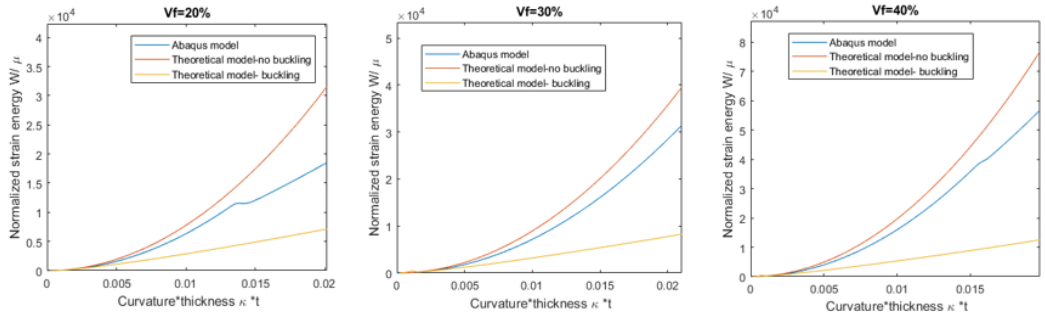

Figure 3.15: Strain energy and moment per width of the matrix.

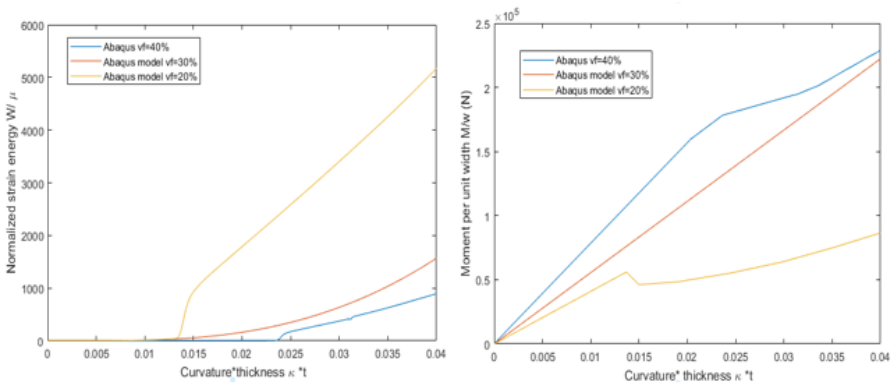

Figure 3.16: Results for different fiber/matrix shear modulus ratios.

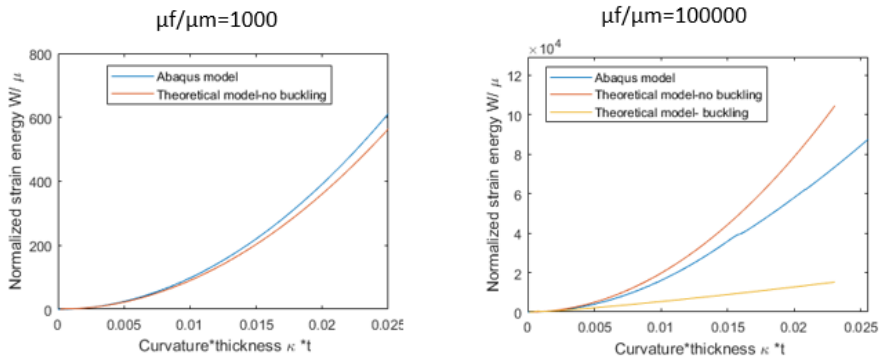

Figure 3.17: Comparison with W. Francis model.

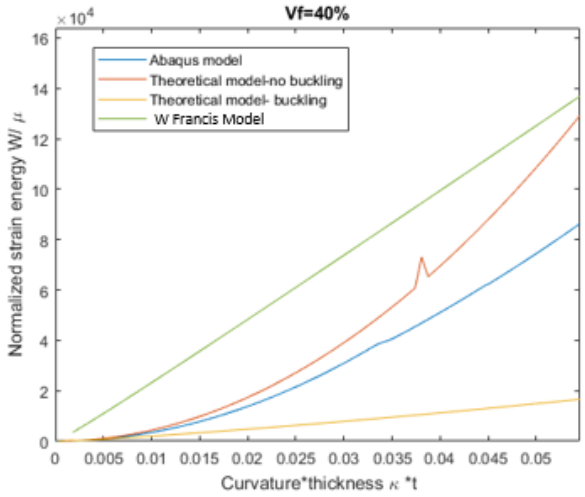

Chapter 4

Summary

4.1 Conclusions

A new energy model has been developed for studying micro-buckling in soft fiber reinforced composites. This new approach includes a large strain formulation and homogenization methods. The definition of the kinematics are based on the mechanical behavior observed in experiments. Some of the kinematic parameters remain as unknowns and they are found by minimizing the strain energy for a given curvature.

Abaqus has been used to run numerical simulation in order to validate the theoretical model. The comparison shows good agreement for the pre-buckling regime. However, the model fails to predict when buckling appears and underestimates significantly the buckling energy. The cause of this difference is still unclear and should be further investigated.

The buckling wavelength is currently constrained by the length of the model. Since it an unknown kinematic parameter it should be treated as one of the variables to be optimized. This might be one source of the error. The optimization process has also been problematic for some cases. For some configurations, only local minimums of the strain energy are found instead of the global minimum. Simplifying the model and reducing the number of variables could help to solve this problem. The function λ_b is particularly increasing the complexity of the calculations because it is minimized as a vector of n-variables. This would also help to reduce the time needed for this calculations which is not practical for the current model.

4.2 Future Work

- While the pre-buckling stage seems to be well captured by the proposed analytical model, the post-buckling strain energy differs from the numerical simulations. Therefore, next steps should include investigating the source of this error. The causes might be related to mistakes in the formulation or in the optimization process.

- The current model is not very efficient because of the high number of variables that have to be optimized. It should be studied if more assumptions can be made to simplify the model and improve the efficiency of the code.

- The microbuckling wave length that minimizes the energy should be included as a variable to be optimized. In the presented results, this parameter has been imposed for both the theoretical and the numerical results. This might be related to the discrepancies observed in the results.

- The numerical model could be also improved by not assuming that the cross sections at the boundaries do not remain flat. Instead of using a kinematic coupling in these areas, periodic conditions could be applied in both surfaces.

Bibliography

[1] William H. Francis. Mechanics of Post-Microbuckled Compliant-Matrix Composites. PhD thesis, University of Colorado at Boulder, 2008.

[2] F. Lopez Jimenez. Modeling of soft composites under three-dimensional loading. Composites, Part B 59:173–180, 2014.

[3] T. W. Murphey, W. H. Francis, L. Davis B, J. Mejia-Ariza, and M. Santer. High strain composites. AIAA Spacecraft Structures Conference, 2015.

[4] Juan M. Mejia-Ariza and Thomas W. Murphey. Ultra-flexible advanced stiffness truss (u-fast) for large solar arrays. 57th AIAA/ASCE/AHS/ASC Structures, Structural Dynamics, and Materials Conference, 2016.

[5] B Walter Rosen. Fiber composite materials. American Society for Metals, Metals Park, Ohio, 37, 1965.

[6] PM Jelf and NA Fleck. Compression failure mechanisms in unidirectional composites. Journal of Composite Materials, 26(18):2706–2726, 1992.

[7] LB Greszczuk. Microbuckling failure of circular fiber-reinforced composites. AIAA Journal, 13(10):1311–1318, 1975.

[8] NA Fleck and B Budiansky. Compressive failure of fibre composites due to microbuckling. In Inelastic deformation of composite materials, pages 235–273. Springer, 1991.

[9] ASD Wang. A non-linear microbuckling model predicting the compressive strength of unidirectional composites. In American Society of Mechanical Engineers, Winter Annual Meeting, San Francisco, Calif, 1978.

[10] T. W. Murphey, T. Meink, and M. M. Mikulas. Some micromechanics considerations of the folding of rigidizable composite materials. 42nd AIAA Structures, Structural Dynamics, and Materials Conference,, Seattle, WA: American Institute of Aeronautics and Astronautics, 2001.

[11] RW Ogden and DG Roxburgh. A pseudo–elastic model for the mullins effect in filled rubber. In Proceedings of the Royal Society of London A: Mathematical, Physical and Engineering Sciences, volume 455, pages 2861–2877. The Royal Society, 1999.

[12] A Dorfmann and Ray W Ogden. A constitutive model for the mullins effect with permanent set in particle-reinforced rubber. International Journal of Solids and Structures, 41(7):1855–1878, 2004.

[13] Pedro Ponte Castaneda and Pierre Suquet. Nonlinear composites. In Advances in applied mechanics, volume 34, pages 171–302. Elsevier, 1997.

[14] P Ponte Castañeda. Exact second-order estimates for the effective mechanical properties of nonlinear composite materials. Journal of the Mechanics and Physics of Solids, 44(6):827–862, 1996.

[15] Pedro Ponte Castañeda. Second-order homogenization estimates for nonlinear composites incorporating field fluctuations: Itheory. Journal of the Mechanics and Physics of Solids, 50(4):737–757, 2002.

[16] Oscar Lopez-Pamies and Martin I. Idiart. Fiber-reinforced hyperelastic soids: a realizable homogenization constitutive theory. Journal of Engineering Mathematics, 68:57–83, 200.

[17] Javier Segurado and Javier LLorca. Computational micromechanics of composites: the effect of particle spatial distribution. Mechanics of materials, 38(8-10):873–883, 2006.

[18] Sreedhar Kari, Harald Berger, Reinaldo Rodriguez-Ramos, and Ulrich Gabbert. Computational evaluation of effective material properties of composites reinforced by randomly distributed spherical particles. Composite Structures, 77(2):223–231, 2007.

[19] Armel Mbiakop, Andrei Constantinescu, and Kostas Danas. An analytical model for porous single crystals with ellipsoidal voids. Journal of the Mechanics and Physics of Solids, 84:436–467, 2015.

[20] Jens Feder. Random sequential adsorption. Journal of Theoretical Biology, 87(2):237–254, 1980.

[21] Einar L Hinrichsen, Jens Feder, and Torstein Jøssang. Geometry of random sequential adsorption. Journal of statistical physics, 44(5-6):793–827, 1986.

[22] F. Lopez Jimenez and S. Pellegrino. Folding of fiber composites with a hyperelastic matrix. International Journal of Solids and Structures, 49:395–407, 2011.

[23] L. M. Kanner and C. O. Horgan. Plane strain bending of strain-stiffening rubber-like rectangular beams. International Journal of Solid and Structures, 45:1713–1729, 2007.

[24] O Pierard, J LLorca, J Segurado, and Issam Doghri. Micromechanics of particle-reinforced elasto-viscoplastic composites: finite element simulations versus affine homogenization. International Journal of Plasticity, 23(6):1041–1060, 2007.